Available online at www.sciencedirect.com
SCIENCE DIRECT®
Journal of Computational Physics 198 (2004) 628–644
JOURNAL OF COMPUTATIONAL PHYSICS
www.elsevier.com/locate/jcp

A lattice Boltzmann method for incompressible two-phase flows with large density differences

T. Inamuro *, T. Ogata, S. Tajima, N. Konishi

Department of Chemical Engineering, Graduate School of Engineering, Kyoto University, Katsura Campus, Kyoto 615-8510, Japan

Received 13 June 2003; received in revised form 20 December 2003; accepted 12 January 2004
Available online 21 February 2004

Abstract

A lattice Boltzmann method for two-phase immiscible fluids with large density differences is proposed. The difficulty in the treatment of large density difference is resolved by using the projection method. The method can be applied to simulate two-phase fluid flows with the density ratio up to 1000. To show the validity of the method, we apply the method to the simulations of capillary waves, binary droplet collisions, and bubble flows. In capillary waves, the angular frequencies of the oscillation of an ellipsoidal droplet are obtained in good agreement with theoretical ones. In the simulations of binary droplet collisions, coalescence collision and two different types of separating collisions, namely reflexive and stretching separations, can be simulated, and the boundaries of the three types of collisions are in good agreement with an available theoretical prediction. In the bubble flows, the effect of mobility on the coalescence of two rising bubbles is investigated. The behavior of many bubbles in a square duct is also simulated.

AMS: 65M99; 76T10

Keywords: Lattice Boltzmann method; Two-phase flow; Capillary wave; Binary droplet collision; Bubble flow

1. Introduction

Recently, the lattice Boltzmann method (LBM) has been developed into an alternative and promising numerical scheme for simulating multicomponent fluid flows. Gunstensen et al. [1] developed a multicomponent LBM based on the two-component lattice gas model. Shan and Chen [2] proposed an LBM model with mean-field interactions for multiphase and multicomponent fluid flows. Swift et al. [3] developed an LBM model for multiphase and multicomponent fluid flows using the free-energy approach. He et al. [4] proposed a new lattice Boltzmann multiphase model using the idea of level-set for multiphase flow.

* Corresponding author. Tel.: +81-75-753-5791; fax: +81-75-761-4947.
E-mail address: inamuro@cheme.kyoto-u.ac.jp (T. Inamuro).

0021-9991/$ - see front matter
doi:10.1016/j.jcp.2004.01.019

Inamuro et al. [5,6] also proposed an LBM for multicomponent immiscible fluids with the same density. Ginzburg and Steiner [7] have proposed a generalized LBM model to simulate free-surface flows by modifying the above model by Gunstensen et al. Tölke et al. [8] also have proposed an LBM for immiscible binary fluids with variable viscosities and density ratios based on the model by Gunstensen et al. and applied the method to the simulation of binary flows through porous media. Sankaranarayanan and Sundaresan [9] and Sankaranarayanan et al. [10,11] have developed an implicit LBM for multicomponent flows based on the above Shan and Chen model and used the method for the analysis of drag, lift, and virtual mass forces in bubbly suspensions. The above LBM models have great advantages over conventional methods for multiphase flows. They do not track interfaces, but can maintain sharp interfaces without any artificial treatments. Also, the LBM is accurate for the mass conservation of each component fluid. While most of the above LBM models for multiphase and multicomponent fluid flows are based on heuristic ideas with no direct connection to kinetic theory, Luo [12,13] and Luo and Girimaji [14,15] have rigorously derived the LBM models for multiphase fluids from the Enskog equation and for multicomponent fluids from the corresponding kinetic equations and provided a unified framework to treat the LBM models for multiphase and multicomponent fluids.

On the other hand, diffuse-interface methods are used for many applications to interfacial phenomena [16–19]. Each of the above LBM models may be regarded as one of the diffuse-interface methods. In the LBM models, the pressure tensor is introduced through the collision term. Since the LBM is classified as a mesoscopic approach to the simulation of fluid dynamics, the combination of LBM and diffuse-interface methods is suitable for the simulation of two-phase fluid flows.

Although the LBM is a promising method for multicomponent fluid flows, one of disadvantages is that all above schemes are limited to small density ratios less than 10 due to the numerical instability in the interface with large density ratios. Usually the density ratio of liquid–gas systems is larger than 100, e.g., the density ratio of water to air is about 1000:1. Thus, the development of an LBM for two-phase fluids with large density ratios is required. Teng et al. [20] used the total variation diminishing with artificial compression (TVD/AC) scheme to the lattice Boltzmann multiphase model in order to stabilize the computation for large density ratios up to 100, but the method has been applied only to the problems with infinitesimal flows such as phase separation. The numerical instability in the interface with large density ratios is mainly caused by spurious velocities near the interface which become larger as the density ratio increases and do not satisfy the continuity equation. In the simulation of flows with large density differences, a key to the problem is to assure the continuity equation near the interface at each time step.

The aim of the present paper is to propose a heuristic LBM for two-phase fluids with large density differences. The difficulty in the treatment of large density differences is resolved by using the projection method [21]. In the projection method the continuity equation in the interfacial region is satisfied at every time step. Two particle velocity distribution functions are used. One is used for the calculation of an order parameter which distinguishes two phases, and the other is used for the calculation of a predicted velocity of the two-phase fluid without a pressure gradient. The current velocity satisfying the continuity equation can be obtained by using the relation between the velocity and the pressure correction which is determined by solving the Poisson equation. In order to show the validity of the method, we apply the method to the simulations of capillary waves, binary droplet collisions, and bubble flows.

The paper is organized as follows. In Section 2 we propose an LBM for two-phase fluids with large density differences and derive governing equations for macroscopic variables by using the asymptotic theory. In Section 3 we present numerical examples, capillary waves, binary droplet collisions, and bubble flows. In capillary waves, the oscillation of an ellipsoidal droplet is calculated. In the simulations of binary droplet collisions, coalescence collision and two different types of separating collisions, namely reflexive and stretching separations, are simulated. In the bubble flows, the effect of mobility on the coalescence of two bubbles is investigated. Concluding remarks are given in Section 4.

2. Numerical method

2.1. Two-phase lattice Boltzmann method

Non-dimensional variables defined in Appendix A are used as in [23]. In the LBM, a modeled fluid, composed of identical particles whose velocities are restricted to a finite set of N vectors $\boldsymbol{c}_i$ ($i = 1, 2, \ldots, N$), is considered. The fifteen-velocity model ($N = 15$) is used in the present paper. The velocity vectors of this model are given by

$$[\boldsymbol{c}_1, \boldsymbol{c}_2, \boldsymbol{c}_3, \boldsymbol{c}_4, \boldsymbol{c}_5, \boldsymbol{c}_6, \boldsymbol{c}_7, \boldsymbol{c}_8, \boldsymbol{c}_9, \boldsymbol{c}_{10}, \boldsymbol{c}_{11}, \boldsymbol{c}_{12}, \boldsymbol{c}_{13}, \boldsymbol{c}_{14}, \boldsymbol{c}_{15}] = \begin{bmatrix} 0 & 1 & 0 & 0 & -1 & 0 & 0 & 1 & -1 & 1 & 1 & -1 & 1 & -1 & -1 \\ 0 & 0 & 1 & 0 & 0 & -1 & 0 & 1 & 1 & -1 & 1 & -1 & -1 & 1 & -1 \\ 0 & 0 & 0 & 1 & 0 & 0 & -1 & 1 & 1 & 1 & -1 & -1 & -1 & -1 & 1 \end{bmatrix}. \tag{1}$$

In the present paper we describe an athermal model for two-phase fluid. Two particle velocity distribution functions, f_i and g_i, are used. The function f_i is used for the calculation of an order parameter which distinguishes two phases, and the function g_i is used for the calculation of a predicted velocity of the two-phase fluid without a pressure gradient. Although we can use any of LBM multiphase models, we use the model by Swift et al. [3] in the present work. The evolution of the particle distribution functions $f_i(\boldsymbol{x}, t)$ and $g_i(\boldsymbol{x}, t)$ with velocity $\boldsymbol{c}_i$ at the point $\boldsymbol{x}$ and at time t is computed by the following equations:

$$f_i(\boldsymbol{x} + \boldsymbol{c}_i\Delta x, t + \Delta t) = f_i(\boldsymbol{x}, t) - \frac{1}{\tau_f}[f_i(\boldsymbol{x}, t) - f_i^{\mathrm{c}}(\boldsymbol{x}, t)], \tag{2}$$

$$g_i(\boldsymbol{x} + \boldsymbol{c}_i\Delta x, t + \Delta t) = g_i(\boldsymbol{x}, t) - \frac{1}{\tau_g}\left[g_i(\boldsymbol{x}, t) - g_i^{\mathrm{c}}(\boldsymbol{x}, t)\right] + 3E_i c_{i\alpha}\frac{1}{\rho}\left[\frac{\partial}{\partial x_\beta}\left\{\mu\left(\frac{\partial u_\beta}{\partial x_\alpha} + \frac{\partial u_\alpha}{\partial x_\beta}\right)\right\}\right]\Delta x, \tag{3}$$

where f_i^{c} and g_i^{c} are functions of Chapman–Enskog type in which the variables $\boldsymbol{x}$ and t enter only through macroscopic variables and/or their derivatives [22], τ_f and τ_g are dimensionless single relaxation times, Δx is a spacing of the cubic lattice, Δt is a time step during which the particles travel the lattice spacing, and the other variables, ρ, μ, and $\boldsymbol{u}$, and constants E_i are defined below. The last term in the right-hand side of Eq. (3) represents the viscous stress tensor divided by the density of the two-phase fluid. In Eqs. (2) and (3), the function f_i^{c} and g_i^{c} are determined so as macroscopic variables satisfy desired equations as shown below. In this sense, the present method is a heuristic LBM for two-phase fluids.

The order parameter ϕ distinguishing two phases and the predicted velocity $\boldsymbol{u}^*$ of the multicomponent fluids are defined in terms of the two particle velocity distribution functions as follows:

$$\phi = \sum_{i=1}^{15} f_i, \tag{4}$$

$$\boldsymbol{u}^* = \sum_{i=1}^{15} \boldsymbol{c}_i g_i. \tag{5}$$

The functions f_i^{c} and g_i^{c} in Eqs. (2) and (3) are given by

$$f_i^{\mathrm{c}} = H_i\phi + F_i\left[p_0 - \kappa_f\phi\frac{\partial^2\phi}{\partial x_\alpha^2} - \frac{\kappa_f}{6}\left(\frac{\partial\phi}{\partial x_\alpha}\right)^2\right] + 3E_i\phi c_{i\alpha}u_\alpha + E_i\kappa_f G_{\alpha\beta}(\phi)c_{i\alpha}c_{i\beta}, \tag{6}$$

$$g_i^{\mathrm{c}} = E_i\left[1 + 3c_{i\alpha}u_\alpha - \frac{3}{2}u_\alpha u_\alpha + \frac{9}{2}c_{i\alpha}c_{i\beta}u_\alpha u_\beta + \frac{3}{2}\left(\tau_g - \frac{1}{2}\right)\Delta x\left(\frac{\partial u_\beta}{\partial x_\alpha} + \frac{\partial u_\alpha}{\partial x_\beta}\right)c_{i\alpha}c_{i\beta}\right] + E_i\frac{\kappa_g}{\rho}G_{\alpha\beta}(\rho)c_{i\alpha}c_{i\beta} - \frac{2}{3}F_i\frac{\kappa_g}{\rho}\left(\frac{\partial\rho}{\partial x_\alpha}\right)^2, \tag{7}$$

where

$$\begin{aligned} &E_1 = 2/9, \quad E_2 = E_3 = E_4 = \cdots = E_7 = 1/9, \\ &E_8 = E_9 = E_{10} = \cdots = E_{15} = 1/72, \\ &H_1 = 1, \quad H_2 = H_3 = H_4 = \cdots = H_{15} = 0, \\ &F_1 = -7/3, \quad F_i = 3E_i (i = 2, 3, 4, \ldots, 15) \end{aligned} \tag{8}$$

and

$$G_{\alpha\beta}(\phi) = \frac{9}{2}\frac{\partial\phi}{\partial x_\alpha}\frac{\partial\phi}{\partial x_\beta} - \frac{3}{2}\frac{\partial\phi}{\partial x_\gamma}\frac{\partial\phi}{\partial x_\gamma}\delta_{\alpha\beta}, \tag{9}$$

with $\alpha, \beta, \gamma = x, y, z$ (subscripts α, β, and γ represent Cartesian coordinates and the summation convention is used). In the above equations, κ_f is a constant parameter determining the width of the interface, κ_g is a constant parameter determining the strength of the surface tension, and $\delta_{\alpha\beta}$ is the Kronecker delta. In Eq. (6), p_0 is given by

$$p_0 = \phi\frac{\partial\psi}{\partial\phi} - \psi = \phi T\frac{1}{1 - b\phi} - a\phi^2 \tag{10}$$

with

$$\psi(\phi, T) = \phi T\ln\left(\frac{\phi}{1 - b\phi}\right) - a\phi^2, \tag{11}$$

where ψ is the bulk free-energy density, and a, b, and T are free parameters determining the maximum and minimum values of the order parameter ϕ. It is noted that f_i^{c} is the same as that of the model by Swift et al. [3] except that Eq. (6) includes no quadratic term of the flow velocity u_α. The last two terms of Eq. (7) represent the effect of interface tension as described below. The term including τ_g represents the negative counterpart of the viscous stress tensor appearing in the original LBM, and this term is needed in order to vanish the original viscous stress tensor. The following finite-difference approximations are used to calculate the first and second derivatives ($\partial\phi/\partial x_\alpha$, $\partial u_\beta/\partial x_\alpha$, $\partial\rho/\partial x_\alpha$, and $\partial^2\phi/\partial x_\alpha^2$) in Eqs. (6), (7) and (9):

$$\frac{\partial\lambda}{\partial x_\alpha} \approx \frac{1}{10\Delta x}\sum_{i=2}^{15} c_{i\alpha}\lambda(\boldsymbol{x} + \boldsymbol{c}_i\Delta x), \tag{12}$$

$$\frac{\partial^2\lambda}{\partial x_\alpha^2} \approx \frac{1}{5\Delta x}\left[\sum_{i=2}^{15}\lambda(\boldsymbol{x} + \boldsymbol{c}_i\Delta x) - 14\lambda(\boldsymbol{x})\right]. \tag{13}$$

The density in the interface is obtained by using the cut-off values of the order parameter, ϕ_{L}^* and ϕ_{G}^*, for the liquid and gas phases with the following relation:

$$\rho = \begin{cases} \rho_{\mathrm{G}}, & \phi < \phi^*_{\mathrm{G}}, \\ \frac{\Delta\rho}{2}\left[\sin\left(\frac{\phi-\overline{\phi^*}}{\Delta\phi^*}\pi\right)+1\right]+\rho_{\mathrm{G}}, & \phi^*_{\mathrm{G}} \leqslant \phi \leqslant \phi^*_{\mathrm{L}}, \\ \rho_{\mathrm{L}}, & \phi > \phi^*_{\mathrm{L}}, \end{cases} \tag{14}$$

where ρ_{G} and ρ_{L} are the density of gas and liquid phases, respectively, $\Delta\rho = \rho_{\mathrm{L}} - \rho_{\mathrm{G}}$, $\Delta\phi^* = \phi^*_{\mathrm{L}} - \phi^*_{\mathrm{G}}$, and $\overline{\phi^*} = (\phi^*_{\mathrm{L}} + \phi^*_{\mathrm{G}})/2$. It is essential to introduce the cut-off values of the order parameter in the present method. The maximum and minimum values of ϕ are changed a little during calculations, and then the change of the density of each phase is magnified in proportion to the density ratio of the two-phase fluid. In order to keep the density of each phase constant, we introduce the cut-off values in the definition of the density of the two-phase fluid.

The viscosity μ in the interface is obtained by

$$\mu = \frac{\rho - \rho_{\mathrm{G}}}{\rho_{\mathrm{L}} - \rho_{\mathrm{G}}}(\mu_{\mathrm{L}} - \mu_{\mathrm{G}}) + \mu_{\mathrm{G}}, \tag{15}$$

where μ_{G} and μ_{L} are the viscosity of gas and liquid phases, respectively. The interfacial tension σ is obtained by

$$\sigma = \kappa_g \int_{-\infty}^{\infty} \left(\frac{\partial\rho}{\partial\xi}\right)^2 \mathrm{d}\xi \tag{16}$$

with ξ being the coordinate normal to the interface [16,26].

It is noted that the flux J_α of the order parameter ϕ is given by

$$J_\alpha = -\theta_{\mathrm{M}}\phi\frac{\partial\mu_{\mathrm{c}}}{\partial x_\alpha} = -\theta_{\mathrm{M}}\frac{\partial P_{\alpha\beta}}{\partial x_\beta}, \tag{17}$$

where θ_{M} is the mobility obtained below, and μ_{c} and $P_{\alpha\beta}$ are the chemical potential and the pressure tensor of the fluid used for the calculation of the order parameter ϕ which are given by

$$\mu_{\mathrm{c}} = \frac{\partial\psi}{\partial\phi} - \kappa_f\frac{\partial^2\phi}{\partial x_\alpha^2}, \tag{18}$$

and

$$P_{\alpha\beta} = \left[p_0 - \kappa_f\phi\frac{\partial^2\phi}{\partial x_\gamma^2} - \frac{\kappa_f}{2}\left(\frac{\partial\phi}{\partial x_\gamma}\right)^2\right]\delta_{\alpha\beta} + \kappa_f\frac{\partial\phi}{\partial x_\alpha}\frac{\partial\phi}{\partial x_\beta}. \tag{19}$$

2.2. Pressure correction

Since $\boldsymbol{u}^*$ is not divergence free ($\nabla\cdot\boldsymbol{u}^* \neq 0$), the correction of $\boldsymbol{u}^*$ is required. The current velocity $\boldsymbol{u}$ which satisfies the continuity equation ($\nabla\cdot\boldsymbol{u} = 0$) can be obtained by using the following equations:

$$Sh\frac{\boldsymbol{u} - \boldsymbol{u}^*}{\Delta t} = -\frac{\nabla p}{\rho}, \tag{20}$$

$$\nabla\cdot\left(\frac{\nabla p}{\rho}\right) = Sh\frac{\nabla\cdot\boldsymbol{u}^*}{\Delta t}, \tag{21}$$

where $Sh = U/c$ is the Strouhal number and p is the pressure of the two-phase fluid. It is noted that $\Delta t = Sh\Delta x$. The Poisson equation (21) can be solved by various methods. In the present paper, we solve Eq. (21) in the framework of LBM. Namely, the following evolution equation of the velocity distribution function h_i is used for the calculation of the pressure p:

$$h_i^{n+1}(\boldsymbol{x} + \boldsymbol{c}_i\Delta x) = h_i^n(\boldsymbol{x}) - \frac{1}{\tau_h}[h_i^n(\boldsymbol{x}) - E_i p^n(\boldsymbol{x})] - \frac{1}{3}E_i\frac{\partial u_\alpha^*}{\partial x_\alpha}\Delta x, \tag{22}$$

where n is the number of iterations and the relaxation time τ_h is given by

$$\tau_h = \frac{1}{\rho} + \frac{1}{2}. \tag{23}$$

The pressure is obtained by

$$p = \sum_{i=1}^{15} h_i. \tag{24}$$

2.3. Algorithm of computation

We now summarize the algorithm of computation.

Step 1. Using Eqs. (2) and (3), compute $f_i(\boldsymbol{x}, t + \Delta t)$ and $g_i(\boldsymbol{x}, t + \Delta t)$, and then compute $\phi(\boldsymbol{x}, t + \Delta t)$ and $\boldsymbol{u}^*(\boldsymbol{x}, t + \Delta t)$ with Eqs. (4) and (5). Also, $\rho(\boldsymbol{x}, t + \Delta t)$ is calculated with Eq. (14).

Step 2. Using Eq. (22) with Eqs. (23) and (24), compute $p(\boldsymbol{x}, t + \Delta t)$. The iteration is repeated until $|p^{n+1} - p^n|/\rho < \varepsilon$ is satisfied in the whole domain.

Step 3. Compute $\boldsymbol{u}(\boldsymbol{x}, t + \Delta t)$ using Eq. (20).

Step 4. Advance one time step and return to Step 1.

It is found in preliminary calculations that using the present method we can simulate multiphase flows with the density ratio up to 1000.

2.4. Governing equations for macroscopic variables

Applying the asymptotic theory [23–25] to Eqs. (2), (3) and (22), we find that the asymptotic expansions of the macroscopic variables with respect to a small parameter $k = \mathrm{O}(\Delta x)$, $\phi' = \phi^{(0)} + k\phi^{(1)}$, $\rho' = \rho^{(0)} + k\rho^{(1)}$, $u'_\alpha = ku_\alpha^{(1)} + k^2u_\alpha^{(2)}$, $p' = k^2p^{(2)} + k^3p^{(3)}$, and $P'_{\alpha\beta} = P_{\alpha\beta}^{(0)} + kP_{\alpha\beta}^{(1)}$ satisfy

$$Sh\frac{\partial\phi'}{\partial t} + u'_\alpha\frac{\partial\phi'}{\partial x_\alpha} = \theta_{\mathrm{M}}\frac{\partial^2 P'_{\alpha\beta}}{\partial x_\alpha\,\partial x_\beta}, \tag{25}$$

$$\frac{\partial u'_\alpha}{\partial x_\alpha} = 0, \tag{26}$$

$$Sh\frac{\partial u'_\alpha}{\partial t} + u'_\beta\frac{\partial u'_\alpha}{\partial x_\beta} = -\frac{1}{\tau_g\rho'}\frac{\partial p'}{\partial x_\alpha} + \frac{1}{\rho'}\frac{\partial}{\partial x_\beta}\left[\mu\left(\frac{\partial u'_\beta}{\partial x_\alpha} + \frac{\partial u'_\alpha}{\partial x_\beta}\right)\right] + \frac{\partial}{\partial x_\beta}\left[\frac{\kappa_g}{\rho'}\left(\frac{\partial\rho'}{\partial x_\alpha}\frac{\partial\rho'}{\partial x_\beta} - \frac{\partial\rho'}{\partial x_\gamma}\frac{\partial\rho'}{\partial x_\gamma}\delta_{\alpha\beta}\right)\right], \tag{27}$$

where θ_{M} is the mobility given by

$$\theta_{\mathrm{M}} = \left(\tau_f - \frac{1}{2}\right)\Delta x. \tag{28}$$

Eq. (25) is the phase-field advection–diffusion equation (the Cahn–Hilliard equation plus advection) for ϕ. Eqs. (26) and (27) are the continuity equation and the Navier–Stokes equations for incompressible two-phase fluid with an interfacial tension, if we choose $\tau_g = 1$. The last term of the right-hand side in Eq. (27) represents the interfacial tension given by Eq. (15).

It is pointed out that large mobilities overly damp flows [19]. The mobility given by Eq. (28) is of $O(\Delta x)$, unless τ_f is close to $1/2$, but as τ_f approaches $1/2$, Eq. (2) becomes unstable due to numerical instability. An idea of decreasing the mobility is to add the term of $E_i C(\partial P_{\alpha\beta}/\partial x_\beta)c_{i\alpha}\Delta x$ to the function f_i^{c} given by Eq. (6), where C is a constant. The mobility θ_{M} in this case is given by

$$\theta_{\mathrm{M}} = \left(\tau_f - \frac{1}{2} - \frac{1}{3}C\right)\Delta x. \tag{29}$$

By choosing a proper value of C, we can decrease the mobility even with $\tau_f = 1$.

3. Numerical examples

To show the validity of the present method, we apply the method to the simulations of capillary waves, binary droplet collisions, and bubble flows.

3.1. Capillary wave

The oscillation of a spherical liquid droplet in a gas phase under the action of capillary force is considered. Initially, an ellipsoidal droplet is placed at the center of a cubic domain. The surface of the droplet is given by $r = R + 0.1R\cos 2\theta$, where r is the distance from the center, R is the radius of the droplet, and θ is the polar angle. The deviation corresponds to the second mode of oscillations. The density ratio of the liquid to the gas is $\rho_{\mathrm{L}}/\rho_{\mathrm{G}} = 50$ ($\rho_{\mathrm{L}} = 50$, $\rho_{\mathrm{G}} = 1$). The viscosities of the droplet and the gas are $\mu_{\mathrm{L}} = 8 \times 10^{-3}\Delta x$ and $\mu_{\mathrm{G}} = 1.6 \times 10^{-4}\Delta x$, respectively. The periodic boundary condition is used on all the sides of the domain. The quarter of the domain is calculated using the symmetry with x and y axes. The quarter domain is divided into a $40 \times 40 \times 80$ cubic lattice. The parameters in Eq. (10) are freely chosen, and for this example their values are $a = 1$, $b = 6.7$, and $T = 3.5 \times 10^{-2}$; it follows that the maximum and minimum values of the order parameter are $\phi_{\max} = 9.714 \times 10^{-2}$ and $\phi_{\min} = 1.134 \times 10^{-2}$. The cut-off values of the order parameter are $\phi_{\mathrm{L}}^* = 9.2 \times 10^{-2}$ and $\phi_{\mathrm{G}}^* = 1.5 \times 10^{-2}$. The other parameters are fixed at $\kappa_f = 0.5(\Delta x)^2$, $\tau_f = 1$, $\tau_g = 1$, $C = 0$, and $\varepsilon = 10^{-5}$. We change the radius of the droplet R and the interfacial tension σ given by Eq. (16).

Table 1
Comparison of calculated angular frequencies $\omega\Delta x$ of the oscillation of the droplet with theoretical ones

R	$\bar{r}$	σ	Theory	Present	Error (%)
$15\Delta x$	$14.43\Delta x$	$0.2038\Delta x$	3.294×10^{-3}	3.162×10^{-3}	−4.0
$20\Delta x$	$19.25\Delta x$	$0.05107\Delta x$	1.070×10^{-3}	1.034×10^{-3}	−3.4
$20\Delta x$	$19.25\Delta x$	$0.2012\Delta x$	2.124×10^{-3}	2.068×10^{-3}	−2.6
$20\Delta x$	$19.25\Delta x$	$0.7797\Delta x$	4.182×10^{-3}	3.957×10^{-3}	−5.4
$25\Delta x$	$24.06\Delta x$	$0.1980\Delta x$	1.508×10^{-3}	1.513×10^{-3}	+0.3

The theoretical angular frequencies are obtained by $\omega\Delta x = \sqrt{8\sigma/\rho_{\mathrm{L}}\bar{r}^3}$, where $\bar{r}$ is the averaged radius of the initial ellipsoidal droplet [27].

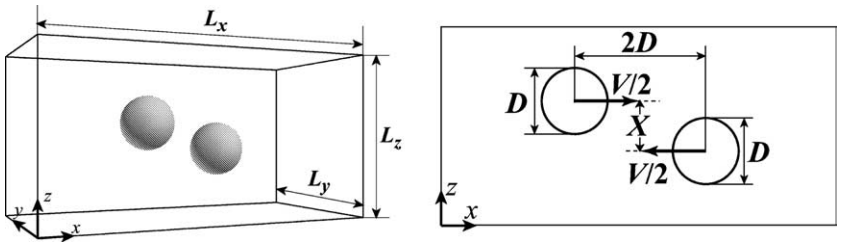

Fig. 1. Computational domain and binary droplet collision.

The angular frequency ω of the oscillation of the droplet is obtained from the time variation of the radius of the droplet. The calculated angular frequencies ω for various R and σ are shown in Table 1 in comparison with the theoretical ones [27]. It is seen from Table 1 that the calculated angular frequencies are in good agreement with the theoretical ones within the errors of 6%.

As for spurious velocities induced in the interface, the maximum velocity in the gas phase is 2.1×10^{-2} for a stationary spherical droplet with $R = 20\Delta x$ and $\sigma = 0.2012\Delta x$ [$\kappa_g = 2.5 \times 10^{-4}(\Delta x)^2$]. Since the width of the interface is thin ($\sim 3\Delta x$) and the interfacial tension is large in this case, the spurious velocities are relatively large. But they do not affect the behavior of the oscillation of the droplet, because the inertia of the gas phase is very small and the oscillation of the droplet is determined only through the ratio between the inertia of the droplet and the interfacial tension. Also, we find that the spurious velocity becomes smaller as the interfacial tension σ decreases and as the lattice points in the interface increase. In numerical examples of bubble flows below, spurious velocities are much smaller than the above case (the maximum

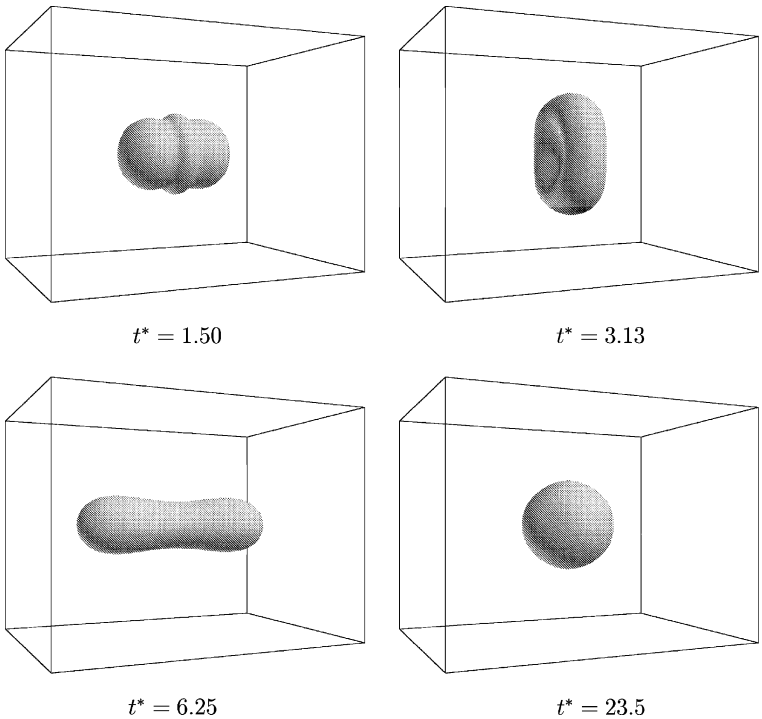

Fig. 2. Time evolution of droplet shape for $We = 20.2$ and $B = 0$ ($t^* = tV/D$).

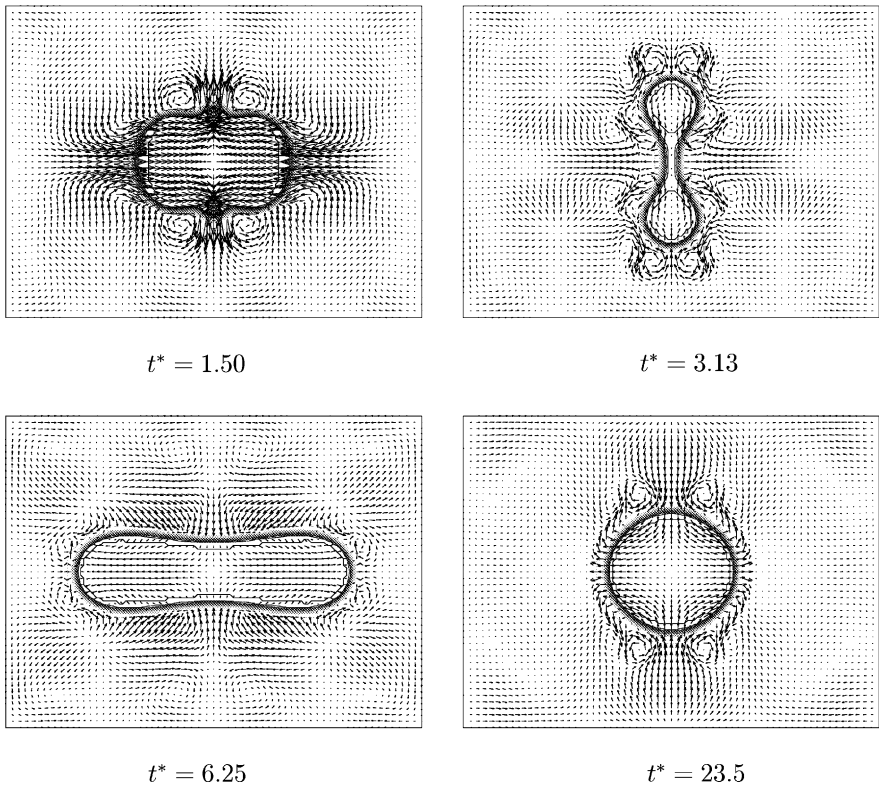

Fig. 3. Time evolution of droplet shape for $We = 20.2$ and $B = 0$ ($t^* = tV/D$).

spurious velocity $< 5 \times 10^{-4}$), since much smaller interfacial tensions are used and slightly more lattice points are distributed in the interface.

3.2. Droplet collision

Two liquid droplets with the same diameter D are placed $2D$ apart in a gas phase, and they collide with the relative velocity V (see Fig. 1). The density ratio of the liquid to the gas is $\rho_L/\rho_G = 50$ ($\rho_L = 50$, $\rho_G = 1$). The viscosities of the droplet and the gas are $\mu_L = 8 \times 10^{-2}\Delta x$ and $\mu_G = 1.6 \times 10^{-3}\Delta x$, respectively. The dimensionless parameters for binary droplet collisions are the Weber number $We = \rho_L DV^2/\sigma$, the Reynolds number $Re = \rho_L DV/\mu_L$, and the impact parameter $B = X/D$, where X is the distance from the center of one droplet to the relative velocity vector placed on the center of the other droplet (see Fig. 1). The periodic boundary condition is used on all the sides of the domain. The half of the domain is calculated using the symmetry with $y = L_y/2$. The half domain is divided into a 192 (or 128) $\times$ 48 $\times$ 96 cubic lattice. The parameters in Eq. (10) are freely chosen, and for this example their values are $a = 1$, $b = 6.7$, and $T = 3.5 \times 10^{-2}$; it follows that the maximum and minimum values of the order parameter are $\phi_{max} = 9.714 \times 10^{-2}$ and $\phi_{min} = 1.134 \times 10^{-2}$. The cut-off values of the order parameter are $\phi_L^* = 9.2 \times 10^{-2}$ and $\phi_G^* = 1.5 \times 10^{-2}$. The other parameters are fixed at $V = 0.1$, $\kappa_f = 0.5(\Delta x)^2$, $\tau_f = 1$, $\tau_g = 1$, $C = 0$, $\varepsilon = 10^{-5}$ and $D = 32\Delta x$, and κ_g is changed in the range of $20 < We < 80$. The Reynolds number is fixed at $Re = 2000$.

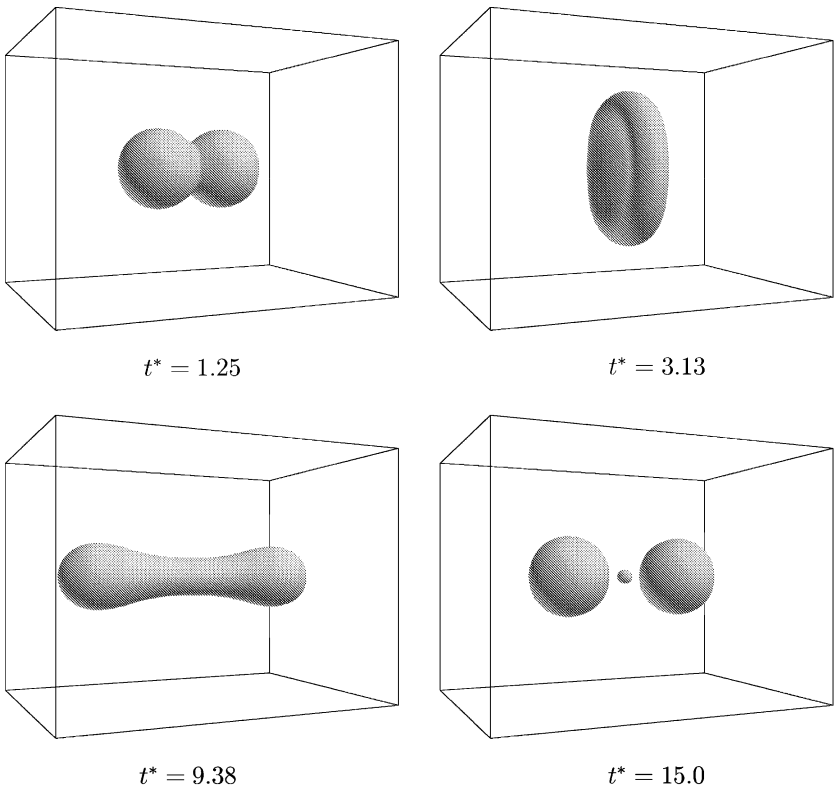

Fig. 4. Time evolution of droplet shape for $We = 39.7$ and $B = 0$ ($t^* = tV/D$).

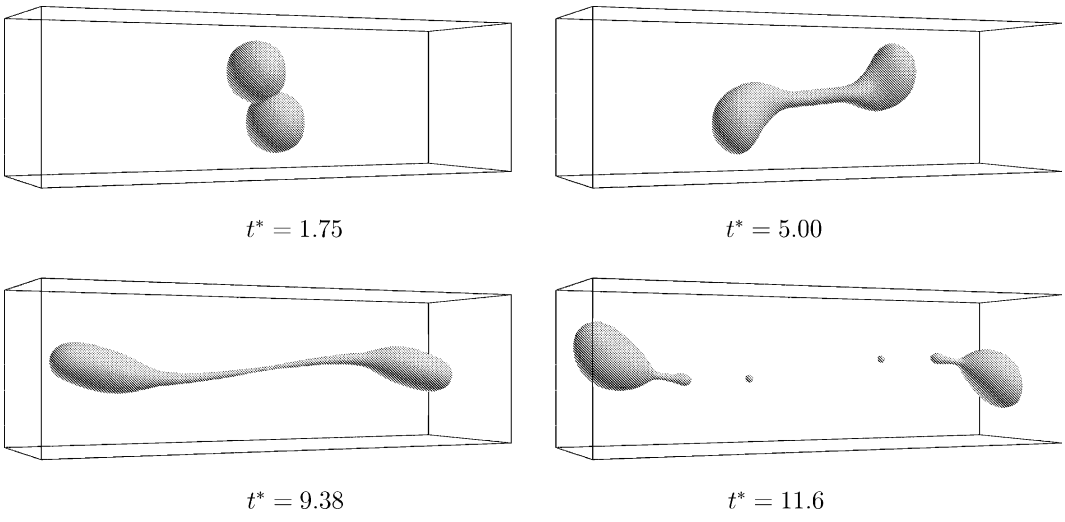

Fig. 5. Time evolution of droplet shape for $We = 79.7$ and $B = 0.813$ ($t^* = tV/D$).

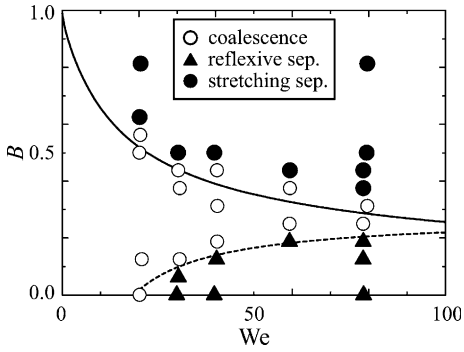

Fig. 6. Calculated results classified into three types of collisions. The solid and broken curves represent the theoretical prediction of the boundaries between three types of collisions [28].

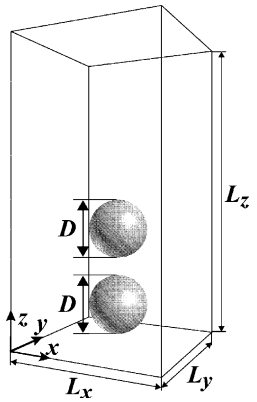

Fig. 7. Computational domain of two rising bubbles.

Fig. 2 shows the calculated results of time evolution of droplet shape for $We = 20.2$ and $B = 0$. After two droplets collide head-on, they form a disk-like droplet. Owing to the large curvature at the circumference of the disk-like droplet, there is a pressure difference between its inner and outer regions caused by surface tension. Thus, the disk contracts radially inward and pushes the liquid outward from its center forming a long cylinder with rounded ends. Then the cylinder oscillates until a spherical droplet is formed. This type of collision is called "coalescence collision". The fluid velocity fields at $y = L_y/2$ are shown in Fig. 3. The complicated gas flows as well as liquid flows inside the droplets are clearly found. Fig. 4 shows the calculated results for $We = 39.7$ and $B = 0$. The time evolution of droplet shape is similar to the previous case up to the formation of a long cylinder with rounded ends. In this case, however, the cylinder breaks into two droplets and a smaller satellite droplet in the middle. This type of collision is called "reflexive separation collision". Fig. 5 shows the calculated results for

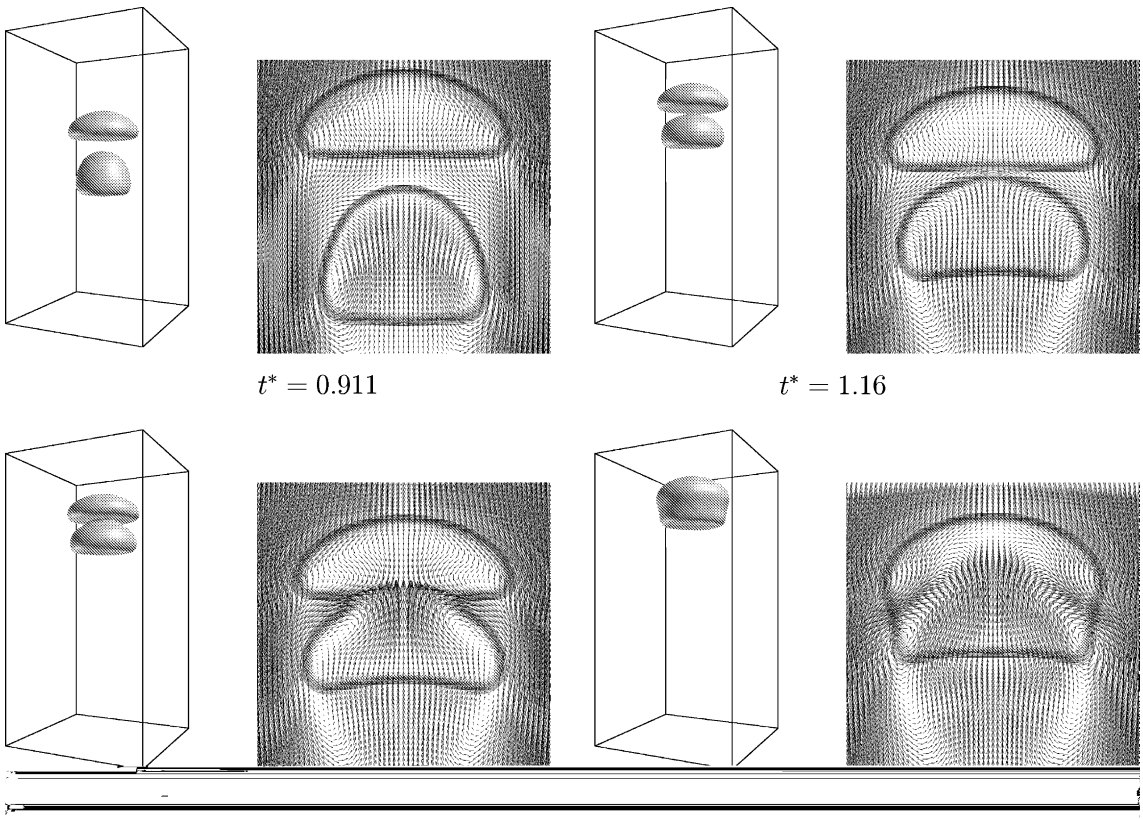

Fig. 8. Time evolution of bubble shapes (left) and velocity vectors and density contours on $y = L_y/2$ (right) for $M = 1 \times 10^{-5}$, $E = 10$, $\rho_L/\rho_G = 50$, and $\theta_M = 0.5\Delta x$ ($t^* = tV/D$, where V is the averaged velocity of gas phase in the lower right result).

$We = 79.7$ and $B = 0.813$. Since the two droplets collide at the high impact parameter, only a portion of them contacts directly, and the remaining portions of the droplets tend to move in the direction of their initial velocities and consequently stretch the region of the interaction. Finally, the droplet breaks into two primary droplets and small satellite droplets. This type of collision is called "stretching separation collision".

The computation time for the case of Fig. 5 required about 47 h on an AMD AthlonXP 1800+ PC machine. The number of iterations in Step 2 of the algorithm of computation is large in a very early stage of calculation due to initial large acceleration (e.g., over 50 iterations were required for $t^* < 1$ in the calculation of Fig. 5), but becomes smaller than 10 after that time. As a result, 51% of the total computation time was spent for Step 2 in this case.

We have calculated the binary droplet collisions for various Weber numbers and impact parameters, and classified the results into the above-mentioned three types of collision in the *We–B* plane as shown in Fig. 6. It is seen that the reflexive separation collisions appear in the region of low impact parameters and high Weber numbers over a critical value, and the stretching separation collisions occur at high impact parameters. The coalescence collisions occur between the two regions. In the figure the theoretical predictions of the boundaries of the three types of collisions [28] are also plotted, and the present calculated results are in good agreement with the theoretical predictions.

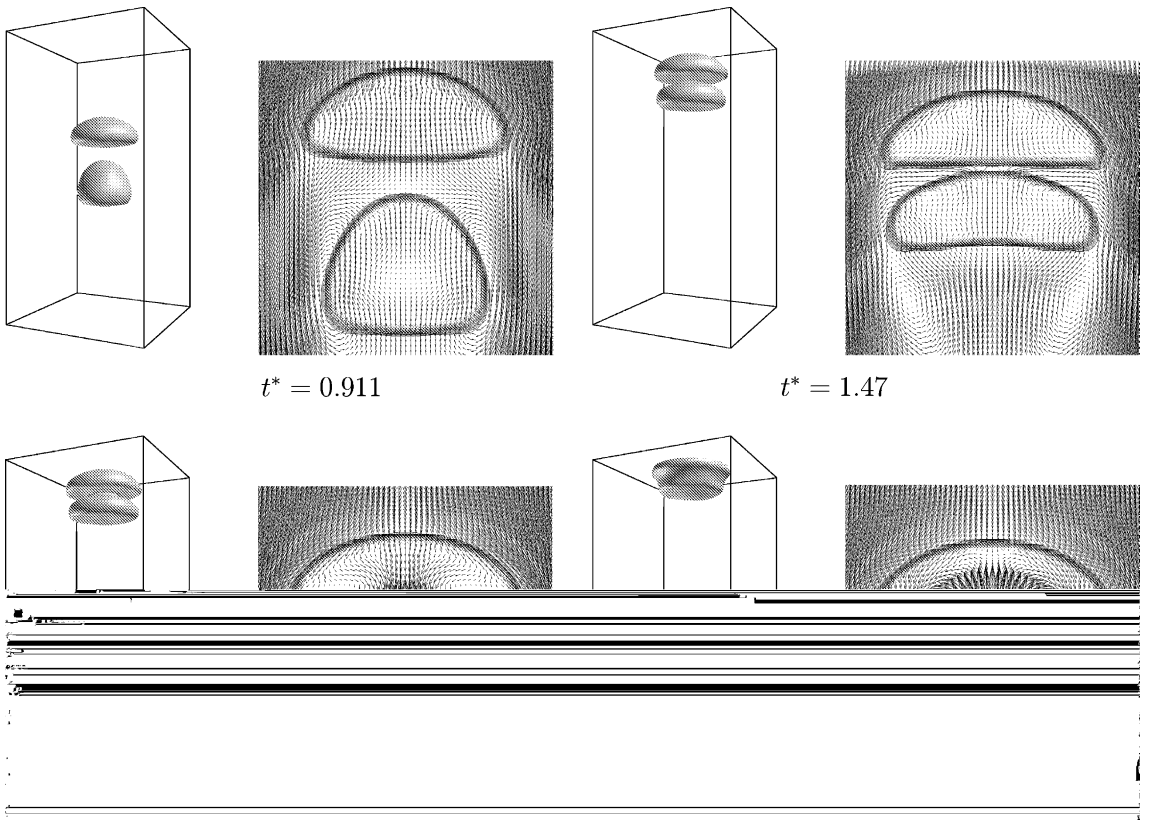

Fig. 9. Time evolution of bubble shapes (left) and velocity vectors and density contours on $y = L_y/2$ (right) for $M = 1 \times 10^{-5}$, $E = 10$, $\rho_L/\rho_G = 50$, and $\theta_M = 0.01\Delta x$ ($t^* = tV/D$, where V is the averaged velocity of gas phase in the lower right result of Fig. 8).

3.3. Bubble flow

First, we calculate the coalescence of two rising bubbles. In the calculation of bubble flows, the gravitational force is considered by adding the term $-3E_i c_{iz}(1 - (\rho_L/\rho))g\Delta x$, where g is the gravitational acceleration to the right-hand side of Eq. (3). Two bubbles with the same diameter D are placed $(4/3)D$ apart in a liquid inside a rectangular domain (see Fig. 7) and is released at time $t = 0$. The density ratio of the liquid to the gas is $\rho_L/\rho_G = 50$ ($\rho_L = 50$, $\rho_G = 1$). The dimensionless parameters for this phenomenon are the Morton number $M = g\mu_L^4(\rho_L - \rho_G)/\rho_L^2\sigma^3$ and the Eötvös number $E = g(\rho_L - \rho_G)D^2/\sigma$. The periodic boundary condition is used on all the sides of the domain. The domain is divided into an $80 \times 80 \times 160$ cubic lattice. The parameters in Eq. (10) for this example are $a = 1$, $b = 1$, and $T = 2.93 \times 10^{-1}$; it follows that the maximum and minimum values of the order parameter are $\phi_{max} = 4.031 \times 10^{-1}$ and $\phi_{min} = 2.638 \times 10^{-1}$. The cut-off values of the order parameter are $\phi_L^* = 3.80 \times 10^{-1}$ and $\phi_G^* = 2.75 \times 10^{-1}$. The other parameters are fixed at $\tau_f = 1$, $\tau_g = 1$, $\varepsilon = 10^{-6}$, $D = 30\Delta x$, $\mu_L/\mu_G = 50$, $\kappa_f = 0.05(\Delta x)^2$ and $\kappa_g = 1 \times 10^{-5}(\Delta x)^2$. The Morton number and the Eötvös number are $M = 1 \times 10^{-5}$ and $E = 10$, respectively. The mobilities of $\theta_M = 0.5\Delta x$ and $0.01\Delta x$ are used.

Figs. 8 and 9 show the calculated results for $\theta_M = 0.5\Delta x$ and $0.01\Delta x$, respectively. It is seen that as the time passes, the lower bubble catches up with the upper bubble. However, if we look at the results carefully, it is seen that the shapes of the lower bubbles for the two cases are different. It is noted that two bubbles

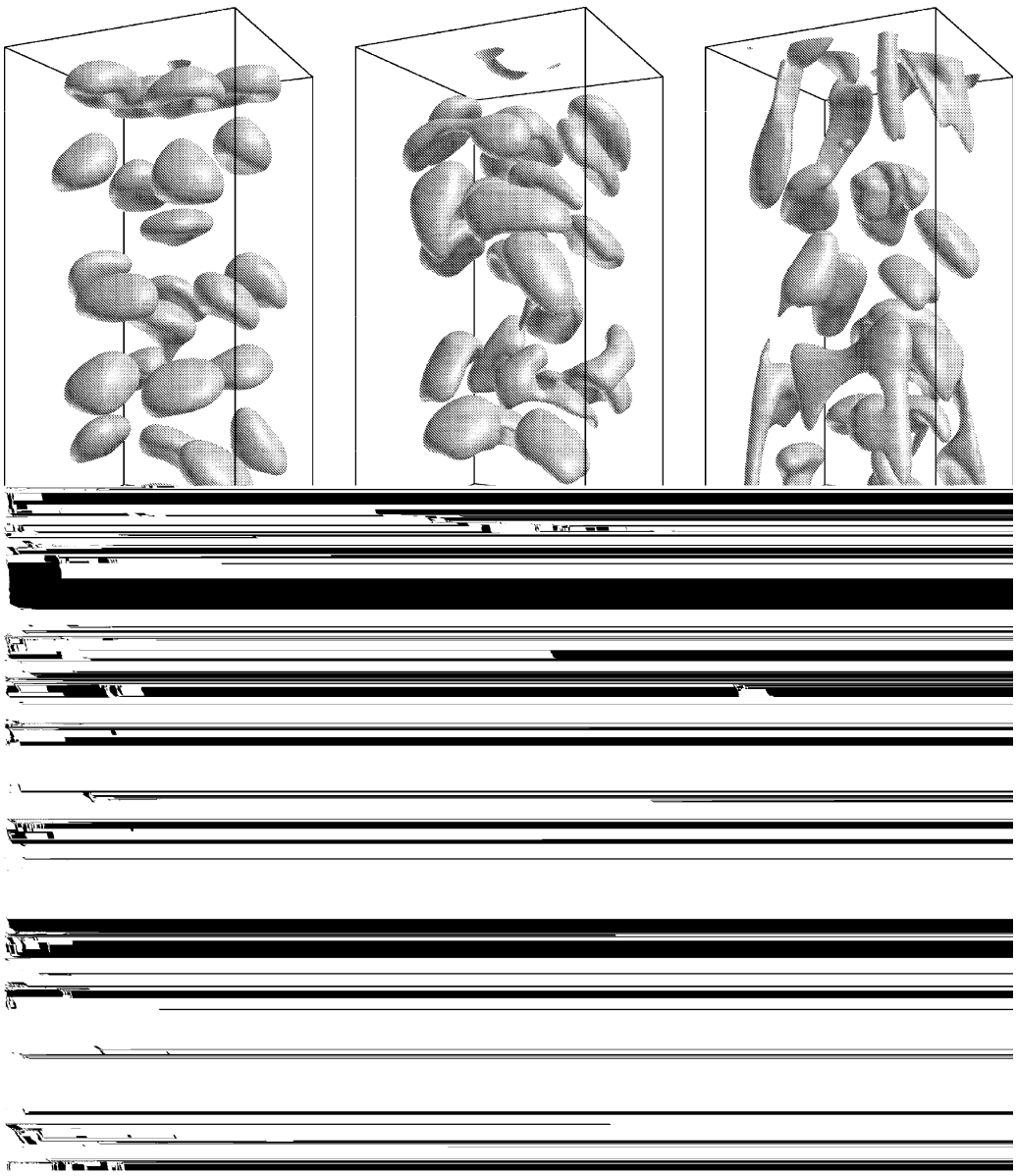

Fig. 10. Time evolution of bubble shapes (upper) and velocity vectors and density contours on $y = L_y/2$ (lower) for $M = 1.7 \times 10^{-11}$, $E = 5$, $\rho_L/\rho_G = 1000$, and $\theta_M = 0.01\Delta x$ ($t^* = tV/D$, where V is the averaged velocity of gas phase in the right result).

coalesce at $t^* = 1.42$ for $\theta_M = 0.5\Delta x$, but two bubbles do not coalesce yet at that time for $\theta_M = 0.01\Delta x$. Namely, it is found that the coalescence phenomena are sensitive to the value of the mobility.

Next, we calculate many bubbles rising in a square duct. Twenty-four bubbles with the same diameter D are placed in a square duct and are released at time $t = 0$. The density ratio is $\rho_L/\rho_G = 1000$ ($\rho_L = 1000$, $\rho_G = 1$). The periodic boundary condition is used on the top and bottom of the domain, and the bounce-back

condition is used on the sides of the domain. The parameters of computation are the same as those used in the previous section except $D = 20\Delta x$, $\kappa_f = 0.08(\Delta x)^2$ and $\kappa_g = 1 \times 10^{-7}(\Delta x)^2$. The Morton number and the Eötvös number are $M = 1.7 \times 10^{-11}$ and $E = 5$, respectively. The mobility is $\theta_M = 0.01\Delta x$.

Fig. 10 shows the calculated results of many bubbles rising in a square duct. It is seen that at $t^* = 1.86$ each bubble goes up and is deformed, and the deformation becomes larger as time goes on. At $t^* = 5.08$ the bubbles coalesce each other, and the interfaces between the gas and liquid phases are deformed into complicated shapes. Note that the complicated flow field can be stably calculated even for the large density ratio of $\rho_L/\rho_G = 1000$. The validation of the results remains in future work.

In addition, we carried out the simulation of a single rising bubble in liquid. The terminal shapes and the terminal Reynolds numbers of the single bubble for various Morton numbers and Eötvös numbers are in good agreement with available experimental data [29].

4. Concluding remarks

A lattice Boltzmann method for two-phase immiscible fluids with large density differences has been developed. The method can simulate two-phase flows with the density ratio up to 1000. In capillary waves, the calculated angular frequencies of the oscillation of an ellipsoidal droplet are in good agreement with theoretical ones within the errors of 6%. In the simulations of binary droplet collisions, the calculated results are in good agreement with an available theoretical prediction. In bubble flows, the complicated unsteady structures of the interface and the velocity field can be stably simulated. Therefore, the method is considered to be a promising method for simulating two-phase flows with large density differences.

The accuracy of the method would depend on the interface width related to the parameter κ_f, the mobility determined by the parameters τ_f and C, and the lattice spacing Δx. Also, the magnitude of spurious velocities in the interface is related to the parameter κ_g and Δx. The study of the accuracy concerning these parameters is required in future work.

Acknowledgements

This work is partly supported by the Grant-in-Aid (No. 12650164) for Scientific Research from the Ministry of Education, Culture, Sports, Science, and Technology in Japan.

Appendix A. Non-dimensional variables

As in [23], we use the following non-dimensional variables defined by a characteristic length L, a characteristic particle speed c, a characteristic time scale $t_0 = L/U$, where U is a characteristic flow speed, a reference order parameter ϕ_0, and a reference density ρ_0:

$$\begin{aligned}
&\hat{\boldsymbol{c}}_i = \boldsymbol{c}_i/c, \quad \hat{\boldsymbol{x}} = \boldsymbol{x}/L, \quad \hat{t} = t/t_0,\\
&\hat{f}_i = f_i/\phi_0, \quad \hat{g}_i = g_i/\rho_0, \quad \hat{h}_i = h_i/(\rho_0 c^2),\\
&\hat{\phi} = \phi/\phi_0, \quad \hat{\rho} = \rho/\rho_0,\\
&\hat{\boldsymbol{u}} = \boldsymbol{u}/c, \quad \hat{p} = p/(\rho_0 c^2),\\
&\hat{\mu} = \mu/(\rho_0 cL), \quad \hat{\sigma} = \sigma/(\rho_0 c^2 L), \quad \hat{\theta}_M = \theta_M/(cL),\\
&\hat{\omega} = \omega L/c, \quad \hat{g} = gL/c^2.
\end{aligned} \tag{A.1}$$

In the computation, we use lattice units with $L = \Delta x$ because of the easiness of programming. The relations of the non-dimensional properties between the two units are as follows:

$$\begin{aligned} &\hat{\mu} = \hat{\mu}_{(L=\Delta x)}\Delta\hat{x}, \quad \hat{\sigma} = \hat{\sigma}_{(L=\Delta x)}\Delta\hat{x}, \quad \hat{\theta}_{\mathrm{M}} = \hat{\theta}_{\mathrm{M}(L=\Delta x)}\Delta\hat{x}, \\ &\hat{\omega}\Delta\hat{x} = \hat{\omega}_{(L=\Delta x)}, \quad \hat{g}\Delta\hat{x} = \hat{g}_{(L=\Delta x)}. \end{aligned} \tag{A.2}$$

Note that the circumflex representing "non-dimensional" in Eqs. (A.1) and (A.2) is omitted in the paper for simplicity.

References

[1] A.K. Gunstensen, D.H. Rothman, S. Zaleski, G. Zanetti, Lattice Boltzmann model of immiscible fluids, Phys. Rev. A 43 (1991) 4320–4327.
[2] X. Shan, H. Chen, Lattice Boltzmann model for simulating flows with multiple phases and components, Phys. Rev. E 47 (1993) 1815–1819.
[3] M.R. Swift, W.R. Osborn, J.M. Yeomans, Lattice Boltzmann simulation of nonideal fluids, Phys. Rev. Lett. 75 (1995) 830–833.
[4] X. He, S. Chen, R. Zhang, A lattice Boltzmann scheme for incompressible multiphase flow and its application in simulation of Rayleigh–Taylor instability, J. Comput. Phys. 152 (1999) 642–663.
[5] T. Inamuro, T. Miyahara, F. Ogino, Lattice Boltzmann simulations of drop deformation and breakup in simple shear flow, in: N. Satofuka (Ed.), Computational Fluid Dynamics 2000, Springer-Verlag, Berlin, 2001, pp. 499–504.
[6] T. Inamuro, R. Tomita, F. Ogino, Lattice Boltzmann simulations of drop deformation and breakup in shear flows, Int. J. Mod. Phys. B 17 (2002) 21–26.
[7] I. Ginzburg, K. Steiner, Lattice Boltzmann model for free-surface flow and its application to filling process in casting, J. Comput. Phys. 185 (2003) 61–99.
[8] J. Tölke, M. Krafczyk, M. Schulz, E. Rank, Lattice Boltzmann simulations of binary fluid flow through porous media, Philos. Trans. R. Soc. Lond. A 360 (2002) 535–545.
[9] K. Sankaranarayanan, S. Sundaresan, Lift force in bubbly suspensions, Chem. Eng. Sci. 57 (2002) 3521–3542.
[10] K. Sankaranarayanan, X. Shan, I.G. Kevrekidis, S. Sundaresan, Analysis of drag and virtual mass forces in bubbly suspensions using an implicit formulation of the lattice Boltzmann method, J. Fluid Mech. 452 (2002) 61–96.
[11] K. Sankaranarayanan, I.G. Kevrekidis, S. Sundaresan, J. Lu, G. Tryggvason, A comparative study of lattice Boltzmann and front-tracking finite-difference methods for bubble simulations, Int. J. Multiphase Flow 29 (2003) 109–116.
[12] L.S. Luo, Unified theory of lattice Boltzmann models for nonideal gases, Phys. Rev. Lett. 81 (1998) 1618–1621.
[13] L.S. Luo, Theory of the lattice Boltzmann method: lattice Boltzmann models for nonideal gases, Phys. Rev. E 62 (2000) 4982–4996.
[14] L.S. Luo, S.S. Girimaji, Lattice Boltzmann model for binary mixtures, Phys. Rev. E 66 (2002) 035301.
[15] L.S. Luo, S.S. Girimaji, Theory of the lattice Boltzmann method: two-fluid model for binary mixtures, Phys. Rev. E 67 (2003) 036302.
[16] J.S. Rowlinson, B. Widom, Molecular Theory of Capillarity, Clarendon Press, Oxford, 1989, pp. 50–68 (Chapter 3).
[17] D.M. Anderson, G.B. McFadden, A.A. Wheeler, Diffuse-interface methods in fluid mechanics, Annu. Rev. Fluid Mech. 30 (1998) 139–165.
[18] B.T. Nadiga, S. Zaleski, Investigations of a two-phase fluid model, Eur. J. Mech. B 15 (1996) 885–896.
[19] D. Jacqmin, Calculation of two-phase Navier–Stokes using phase-field modeling, J. Comput. Phys. 155 (1999) 96–127.
[20] S. Teng, Y. Chen, H. Ohashi, Lattice Boltzmann simulation of multiphase fluid flows through the total variation diminishing artificial compression scheme, Int. J. Heat Fluid Flow 21 (2000) 112–121.
[21] A.J. Chorin, Numerical solution of the Navier–Stokes equations, Math. Comput. 22 (1968) 745–762.
[22] Y. Sone, Kinetic Theory and Fluid Dynamics, Birkhäuser, Boston, 2002, pp. 315–326 (Appendix C).
[23] T. Inamuro, M. Yoshino, F. Ogino, Accuracy of the lattice Boltzmann method for small Knudsen number with finite Reynolds number, Phys. Fluids 9 (1997) 3535–3542.
[24] Y. Sone, Asymptotic theory of flow of rarefied gas over a smooth boundary II, in: D. Dini (Ed.), Rarefied Gas Dynamic, vol. 2, Editrice Tecnico Scientifica, Pisa, 1971, pp. 737–749.
[25] Y. Sone, Asymptotic theory of a steady flow of a rarefied gas past bodies for small Knudsen numbers, in: R. Gatignol, Soubbaramayer (Eds.), Advances in Kinetic Theory and Continuum Mechanics, Springer, Berlin, 1991, pp. 19–31.
[26] T. Inamuro, N. Konishi, F. Ogino, A Galilean invariant model of the lattice Boltzmann method for multiphase fluid flows using free-energy approach, Comput. Phys. Commun. 129 (2000) 32–45.

[27] L.D. Landau, E.M. Lifshitz, Fluid Mechanics, second ed., Pergamon Press, Oxford, 1987, pp. 244–247 (Chapter VII).
[28] N. Ashgriz, J.Y. Poo, Coalescence and separation in binary collisions of liquid drops, J. Fluid Mech. 221 (1990) 183–204.
[29] T. Inamuro, T. Ogata, F. Ogino, Numerical simulation of bubble flows by the lattice Boltzmann method, Future Generation Computer Systems (in press).